π-Electronic Co-crystal Microcavities with Selective Vibronic-Mode Light Amplification: Toward Förster Resonance Energy Transfer Lasing

Daichi Okada,[†] Stefano Azzini,[§] Hiroki Nishioka,[‖] Anna Ichimura,[‖] Hayato Tsuji,[‖,⊥] Eiichi Nakamura,[‖] Fumio Sasaki,[#] Cyriaque Genet,[§] Thomas W. Ebbesen,[§] and Yohei Yamamoto*[,†,‡]

[†]Division of Materials Science, Faculty of Pure and Applied Sciences and [‡]Tsukuba Research Center for Energy Materials Science (TREMS), University of Tsukuba, 1-1-1 Tennodai, Tsukuba, Ibaraki 305-8573, Japan

[§]ISIS & icFRC, Université de Strasbourg and CNRS, 8 allée Gaspard Monge, Strasbourg 67000, France

[‖]Department of Chemistry, The University of Tokyo, Hongo, Bunkyo-ku, Tokyo 113-0033, Japan

[⊥]Department of Chemistry, Faculty of Science, Kanagawa University, 2946 Tsuchiya, Hiratsuka 259-1293, Japan

[#]Electronics and Photonics Research Institute, National Institute of Advanced Industrial Science and Technology (AIST), 1-1-1 Umezono, Tsukuba, Ibaraki 305-8568, Japan

S *Supporting Information*

ABSTRACT: π-conjugated organic microcrystals often act as optical resonators in which the generated photons in the crystal are confined by the reflection at the crystalline facets and interfere to gain lasing action. Here, we fabricate microcrystals from a mixture of carbon-bridged oligo-*para*-phenylenevinylenes (COPVs) with energy-donor (D) and energy-acceptor (A) characters. Upon weak excitation of the single D−A co-crystal, Förster resonance energy transfer (FRET) takes place, exhibiting spontaneous emission from A. In contrast, upon strong pumping, stimulated emission occurs before FRET, generating lasing action from D. Lasing occurs with single- and dual-vibronic levels, and the lasing wavelength can be modulated by the doping amount of A. Time-resolved spectroscopic studies reveal that

the rate constant of lasing is more than 20 times greater than that of FRET. Furthermore, microcrystals, vertically grown on a Ag-coated substrate, reduce the lasing threshold by one-fourth. This study proposes possible directions toward organic solid FRET lasers with microcrystalline resonators.

KEYWORDS: *Microlaser, FRET, organic crystal, resonator, kinetics*
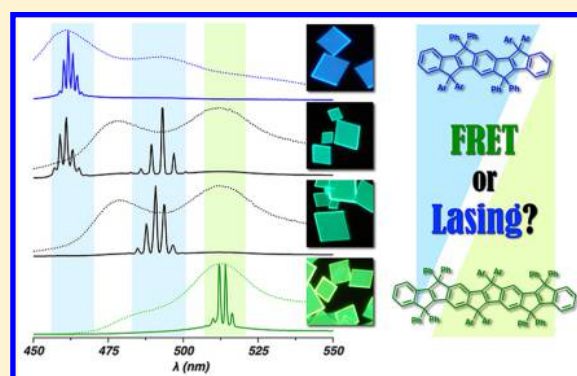
Microcrystals often work as optical and laser resonators in which the crystalline facets act as feedback mirrors and generated photons are confined in the crystal by the internal reflection.[1−3] Microcrystals from π-conjugated molecules offer the advantage of semiconducting properties as well as the possibilities of controlling shape, molecular order, and orientation. For organic lasers, microcrystalline resonators can be afforded by a simple crystallization process from solution. Förster resonance energy transfer (FRET) is expected to have advantages for obtaining lasing action with high efficiency; it possibly yields low-threshold lasing by harvesting light and transferring it from an energy donor (D) to an acceptor (A) molecule. Several types of FRET-assisted lasers have been reported: random lasers from core−shell colloids,[4−7] optofluidic dye lasers in microtube cavities coupled with whispering gallery mode (WGM),[8−10] and vertical cavity surface emitting lasers (VCSELs) from host−guest mixing molecular system.[11] However, there are no reports of FRET-

assisted lasing from solid microcrystalline resonators composed of organic molecules. One reason is referred to the difficulty in a preparation of microcrystals made of two different molecular components with desired composition.

In this Letter, we pursue the possibility of FRET lasers with microcrystalline cavities. For this purpose, preparation of high-quality faceted microcrystals composed of a D−A mixture is necessary. We find that two carbon-bridged oligo-phenylenevinylenes (COPVs) with D and A characters self-assemble to form micrometer-sized, faceted co-crystals with a variety of the mixing ratio. We first anticipate that energy transfer and subsequent lasing take place upon optical pumping. Indeed, upon weak excitation, FRET takes place with high efficiency, leading to photoluminescence (PL) from A. However, upon
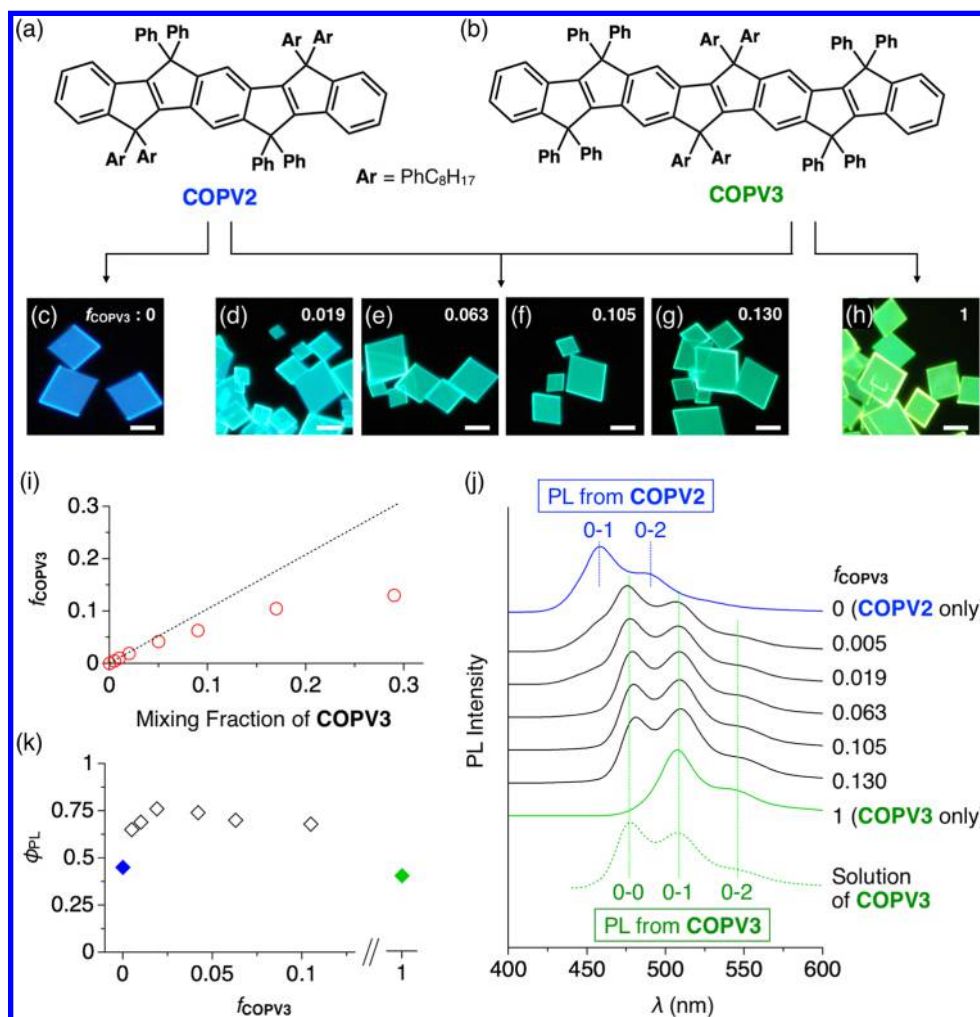
Figure 1. (a, b) Molecular structures of (a) **COPV2** and (b) **COPV3**. (c–h) Fluorescent micrographs of microcrystals of (c) **COPV2** and (h) **COPV3** and co-crystals with f_{COPV3} = (d) 0.019, (e) 0.063, (f) 0.105, and (g) 0.130. Scale bars: 10 μm. λ_{ex} = 350−390 nm. (i) Plot of f_{COPV3} vs mixing fraction of **COPV3** in the preparation process. The dashed line indicates the level if **COPV2** and **COPV3** co-assemble homogeneously without segregation. (j) Steady-state PL spectra of thin films of microcrystals of **COPV2** and **COPV3** with f_{COPV3} = 0 (blue), 0.005−0.13 (black) and 1 (green), and that of a CHCl$_3$ solution of **COPV3**. λ_{ex} = 380 nm. (k) Plot of ϕ_{PL} of the microcrystals vs f_{COPV3}. λ_{ex} = 380 nm.

strong pumping, stimulated emission from D occurs much faster than FRET. Time-resolved studies reveal that the rate constant of lasing is more than 20 times greater than that of FRET. Changing the D-to-A ratio can modulate the lasing wavelength and further achieves dual-color lasing. The lasing threshold is reduced by one-fourth when using microcrystals grown vertically on a Ag-coated substrate.

The molecules used in this study are **COPV2** and **COPV3**, composed of two and three COPV units, respectively (Figure 1a,b).[12−16] These molecules possess rigid π-conjugated planes isolated by aryl side chains in the crystalline lattice.[12] As a result, these molecules have high stability against photo-irradiation and function as gain media for distributed feedback lasers.[13,15,16] As previously reported,[12] CHCl$_3$ solutions of **COPV2** and **COPV3** show photoabsorption maxima (λ_{abs}) at 397 and 436 nm, respectively, with their corresponding PL maxima (λ_{em}) at 457 and 478 nm with the PL quantum yield (ϕ_{PL}) of near-unity (Figure S1a,b).[12] The PL band of **COPV2** largely overlaps with the photoabsorption band of **COPV3**; therefore, FRET can occur from **COPV2** to **COPV3**.

Microcrystals of **COPV2**, **COPV3**, and their co-crystals were prepared by surface self-assembly on a quartz substrate by slow

evaporation of the solvent from their solutions (mole fraction of the mixed **COPV3**: 0, 0.005, 0.01, 0.02, 0.05, 0.09, 0.17, 0.29, and 1; for details, see the Supporting Information and Figure S2). The crystals obtained have a rhombic, plate-like morphology with the side length (L) of 4−35 μm and the height (h)-to-L ratio of around 1/10 (Figures S3 and S4). Under illumination at λ_{ex} = 350−390 nm, the microcrystals of **COPV2** display blue-colored PL (Figure 1c). As the mixing fraction of **COPV3** increases, the PL color of the co-crystals shifts to bluish-green (Figure 1d−g) and the microcrystals of **COPV3** display green-colored PL (Figure 1h). Photo-absorption spectroscopy of the dissolved microcrystals reveals that the actual mole fraction of doped **COPV3** (f_{COPV3}) deviates from the ideal value as mixing fraction of **COPV3** increases (Figures 1i and S5).

The packing structure of **COPV2** is revealed by single-crystal X-ray diffraction (XRD) analysis (Figure S6a−c and Table S1). The crystal system is monoclinic with the space group $P2_1/n$. The π-conjugated plane of COPV is nearly isolated with one another, separated by their side chains.[12] Powder XRD pattern of the microcrystalline platelets of **COPV2** grown on a substrate shows a series of intense
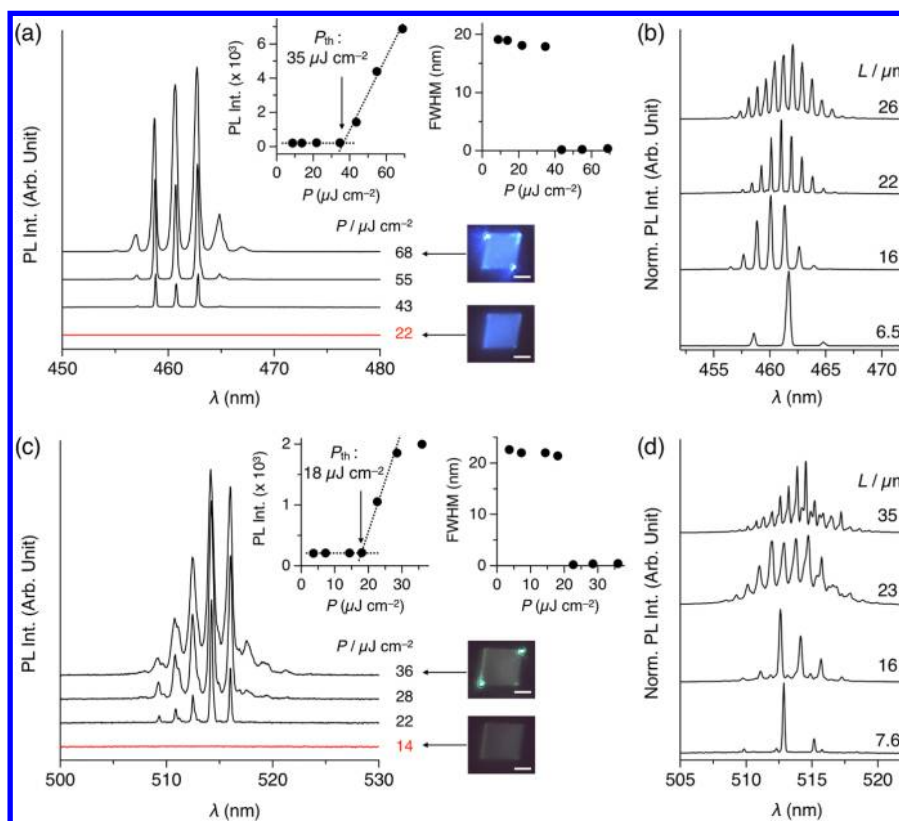
Figure 2. (a, c) PL spectra of microcrystals of (a) **COPV2** and (c) **COPV3** upon femtosecond pumping with different power density, along with fluorescent micrographs below and above P_{th}. Insets show plots of PL intensity (left) and fwhm (right) vs pumping power density. Scale bars: 5 μm. (b, d) PL spectra of microcrystals of (b) **COPV2** and (d) **COPV3** upon femtosecond pumping with different crystal sizes.

diffraction peaks with Miller indices of (1 0−1), (2 0−2), and (3 0−3), indicating that the π-conjugated plane of COPV forms an face-on orientation on the substrate surface (Figure S6d). Similarly, microcrystalline platelet on a substrate with f_{COPV3} = 0.042, 0.063, and 0.105 display XRD patterns almost identical with that of **COPV2** (Figure S6d). However, the full-width at the half-maximum (fwhm) of the diffraction peaks at 2θ = 5.79° increases from 0.09° (f_{COPV3} = 0) to 0.135° (f_{COPV3} = 0.105), indicating that the crystallinity reduces with increasing the doping level of **COPV3** (Figure S6e). In addition, a weak diffraction peak derived from crystal of **COPV3** was observed in the XRD pattern of microcrystals with f_{COPV3} = 0.063 and 0.105, indicating that the resultant powders contain both the co-crystals of **COPV2** and **COPV3** and crystals of **COPV3**.[17,18] As observed by optical and fluorescence microscopies, rhombic-shaped co-crystals of **COPV2** and **COPV3** and irregular aggregates of **COPV3** precipitated separately on the substrate (Figure S7). There are examples of D−A mixtures with variable doping levels in organic thin films prepared by the coevaporation and codeposition method in the gas phase.[11,17,18] However, co-crystallization with a variable doping ratio in a solution process is very rare. The similarity of the molecular structures of **COPV2** and **COPV3** possibly enables their co-crystallization during slow evaporation of an acetone−DMF cosolvent (Figure S2).

Upon photoexcitation with stationary light at λ_{ex} = 380 nm, the microcrystals of pure **COPV2** and **COPV3** barely show the 0−0 vibronic-level PL band due to self-absorption (Figure S1c,d). In contrast, microcrystals with f_{COPV3} from 0.005 to 0.13 show almost-identical PL spectra as that of a solution of

COPV3 with 0−0, 0−1, and 0−2 bands at 476, 506, and 545 nm, respectively (Figure 1j). These results indicate that **COPV3** is molecularly dispersed in the medium of **COPV2** and FRET takes place efficiently from **COPV2** to **COPV3** in the microcrystals. Because of the suppression of concentration quenching, the ϕ_{PL} of the co-crystals (0.65−0.76) is much higher than those of the microcrystals of pure **COPV2** (0.45) and pure **COPV3** (0.40; Figure 1k and Table S2).

Upon femtosecond (fs) pumping of a single microcrystal, lasing occurs above the pumping threshold, P_{th} (λ_{ex} = 397 nm, Δ = 300 fs, and f = 1 kHz; for details, see Figure S8).[19] A whole single microcrystal was excited by femtosecond-laser pulses from the incident angle of 60° with respect to the vertical direction of the substrate (irradiation spot: $\phi \approx$ 60 μm). Microcrystals of pure **COPV2** and **COPV3** display lasing peaks at around 460 and 510 nm with P_{th} of 35 and 18 μJ cm^{-2}, respectively (Figure 2a,c). Above P_{th}, fwhm of the PL peaks become narrow (∼0.2 nm; Figure 2a and c, inset). The mode spacing ($\Delta\lambda$) become small as the size of the crystal increases (Figure 2b,d), indicating that the microcrystals act as an optical resonator. Because the corners of the crystal emit bright luminescence upon pumping above P_{th} (Figure 2a,c, inset), the resonant mode is expected as a circulation mode.[20] By two-dimensional finite-difference time-domain (2D-FDTD) simulations using refractive index value of a thin film of **COPV2** (Figure S9e), several resonator modes are assumed such as quasi-WGM and Fabry−Pérot (F−P) mode (panels a and b of Figure S9, respectively).[21,22] Among them, quasi-WGM is the most plausible because the Q-factor of a peak at ∼460 nm for quasi-WGM (3400, Figure S9c) is much greater than that for F−P mode (310, Figure S9d). It is worth noting
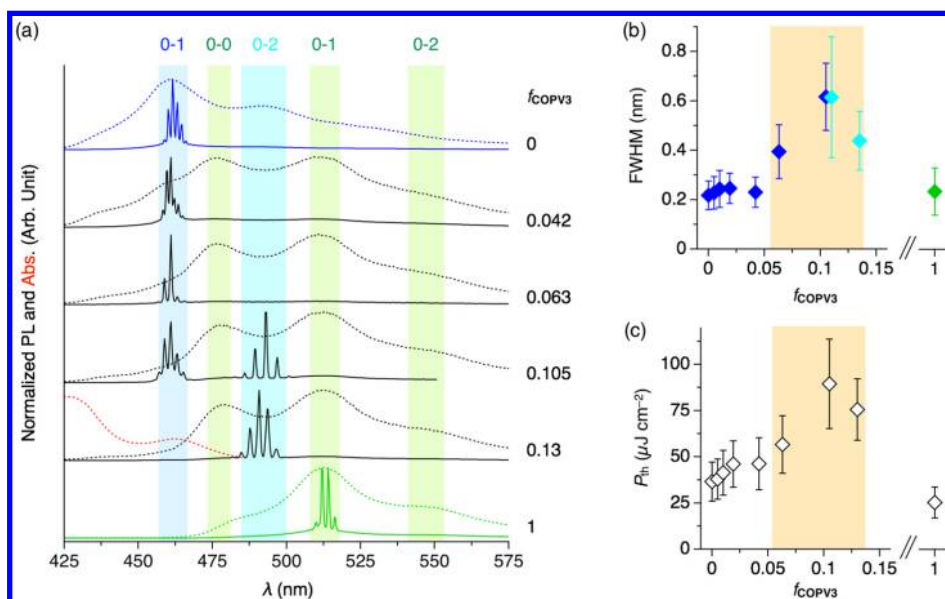
Figure 3. (a) PL spectra of a single microcrystal of **COPV2** and **COPV3** with $f_{COPV3} = 0$ (blue), 0.042−0.13 (black), and 1 (green) upon femtosecond excitation with weak pumping below P_{th} (broken curves) and strong pumping above P_{th} (solid curves). Red broken curve indicate photoabsorption spectrum of the co-crystal with $f_{COPV3} = 0.13$. (b) Plots of fwhm of the lasing peaks at 460 nm (blue), 490 nm (light blue), and 510 nm (green) vs f_{COPV3}. (c) Plot of average P_{th} vs f_{COPV3}.

that the microcrystals of **COPV2** and **COPV3** are highly stable against the optical pumping;[13] the number of the pump pulses (pp) at which the PL intensity decreases to the half from the initial value reaches 4.0×10^5 and 2.1×10^6 pp for microcrystals of **COPV2** and **COPV3**, respectively (Figure S10).

However, co-crystals of **COPV2** and **COPV3** display lasing in the 0−1 PL wavelength region of **COPV2**, not in that of **COPV3** via FRET, even when f_{COPV3} increases to 0.063 (Figures 3a and S11a−c). When f_{COPV3} increases to 0.105, lasing occurs in both the 0−1 and 0−2 PL regions of **COPV2** (Figures 3a and S11d). The further increase of f_{COPV3} to 0.13 results in lasing in the 0−2 wavelength region of **COPV2** without FRET (Figures 3a and S11e). Because the photo-absorption edge of **COPV3** in **COPV2** in the microcrystals is ~480 nm (Figure S12), which overlaps the 0−1 emission from **COPV2** (Figure 3a, red), 0−1 lasing from **COPV2** is subject to a serious reabsorption loss by **COPV3**, leading to only 0−2 lasing from **COPV2**. Optimizing the doping level precisely controls the lasing wavelength, which is advantageous compared with previous reports on dual-color lasing from organic materials.[23−25]

Reabsorption by **COPV3** clearly affects the fwhm of the lasing peaks (Figure 3b).[26,27] At $f_{COPV3} \leq 0.042$, fwhm is around 0.2 nm. fwhm increases as f_{COPV3} increases and reaches ~0.6 nm in the dual-color lasing with $f_{COPV3} = 0.105$. Concomitantly, P_{th} also increases due to reabsorption loss, which reaches 90 μJ cm^{-2} in dual-color lasing with $f_{COPV3} = 0.105$ (Figure 3c).

The time scales of FRET and lasing are investigated by time-resolved studies of cast films of the microcrystals. Upon weak excitation below P_{th}, the PL lifetime (τ) from **COPV2** ($\lambda_{em} = 445$ nm, emission from **COPV2**) decreases from 550 to 280 ps as f_{COPV3} increases from 0 to 0.105 (Figures 4a,c (blue) and S13 and Table S3). However, τ from **COPV3** ($\lambda_{em} = 510$ nm, emission from **COPV3**), via FRET from **COPV2**, is around 1200 ps at $f_{COPV3} = 0.019−0.105$ (Figures 4b,c green and S14
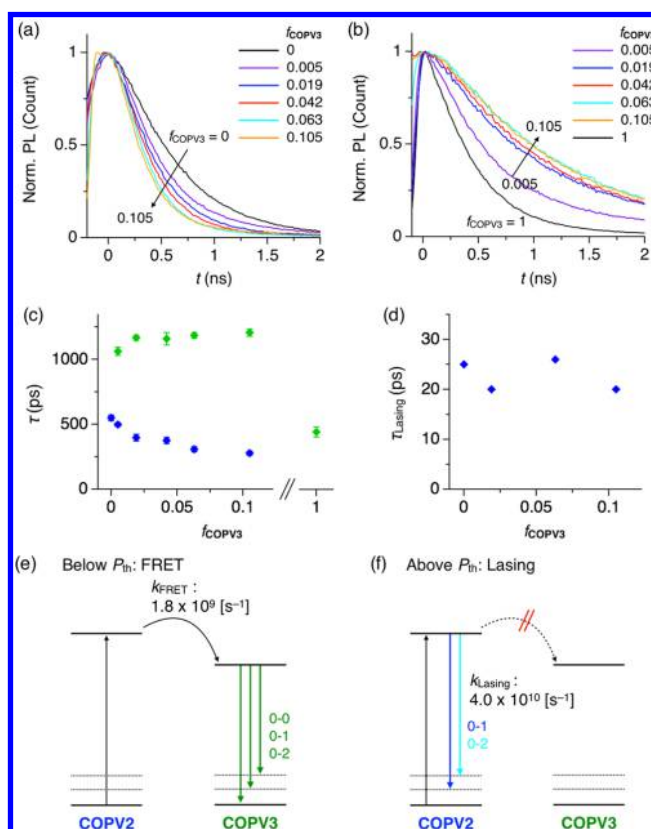

Figure 4. (a, b) PL decay profiles at (a) 445 and (b) 510 nm for thin films of the microcrystals of **COPV2** and **COPV3** with picosecond laser pumping. (c) Plots of τ at $\lambda_{em} = 445$ (blue) and 510 nm (green) and vs f_{COPV3} upon weak pumping by picosecond laser. Error bars show standard deviation from three to five single microcrystals. (d) Plots of τ_{Lasing} at $\lambda_{\Delta abs} = 675$ nm (green) vs f_{COPV3} upon strong pumping by femtosecond laser. (e, f) Schematic representations of the energy diagram and emission mechanism upon excitation (e) below and (f) above P_{th}.
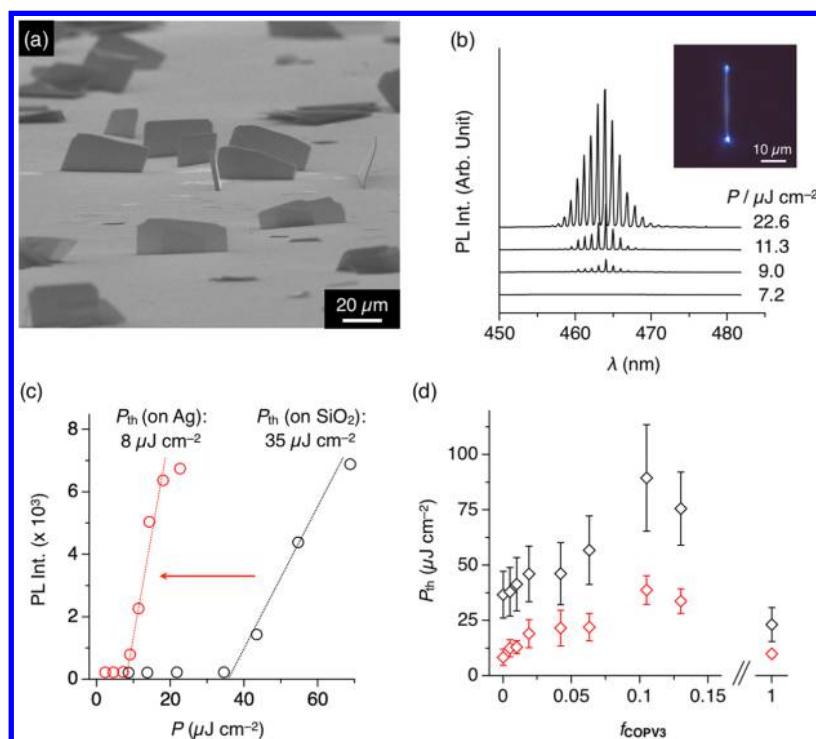
Figure 5. (a) SEM micrograph of the microcrystals grown on a Ag-covered SiO$_2$ substrates (tilted angle: 75°). (b) PL spectra of a vertically grown microcrystal of **COPV2** with different *P*. Inset shows fluorescent microscopy image of a vertically grown microcrystal of **COPV2** upon femtosecond pumping. (c) Plots of PL intensities vs *P* for a microcrystal of **COPV2** grown on SiO$_2$ (black) and Ag-covered SiO$_2$ substrates (red). (d) Plots of average P_{th} vs f_{COPV3} for microcrystals with face-on (black) and edge-on (red) geometries.

and Table S4).[28] The PL decay curves are well-fitted with double or triple exponentials, not single exponentials, indicating that the system is not a single dipole type. It might further indicate that **COPV3** is doped without an ordered orientation. From these results, the rate constant of FRET, k_{FRET} (equal to $1/\tau_{DA} - 1/\tau_D$, where τ_{DA} and τ_D indicate τ at $f_{COPV3} = 0.105$ and 0, respectively), is evaluated as 1.8×10^9 s^{-1}. The FRET efficiency (= $k_{FRET} \times \tau_{DA}$) is then evaluated as ~0.50.

In contrast, upon strong pumping above P_{th}, the rate constant of lasing (k_{Lasing}) is much greater than k_{FRET}. For this purpose, the transient absorption spectroscopy (TAS) method is adopted to evaluate the lifetime of lasing (τ_{Lasing}). In the TAS of **COPV2**, negative and positive Δabs are observed at 460 and 500−750 nm, respectively, originating from laser emission and absorption from the excited state of **COPV2** (Figure S15). The τ_{Lasing} value, evaluated with Δabs of the excited species of **COPV2** at $\lambda = 695$ nm, is 25 ps. (In the pump-and-probe measurement, the probe pulse induces stimulated emission, which makes it difficult to evaluate τ from Δabs at the lasing wavelength, $\lambda = 460$ nm.) Even in co-crystals with $f_{COPV3} = 0.042−0.105$, τ yields almost constant values (20−26 ps; Figure 4d and Table S5). From these results, k_{Lasing} (= $1/\tau_{Lasing}$) is evaluated as ~4.0×10^{10} s^{-1}, which is more than 20 times greater than k_{FRET} (Figure 4e,f).[29]

Rates shown in eqs 1 and 2 are considered for the decay processes of the excited states of **COPV2** and **COPV3**:[11]

$$dN_D/dt = -k_D N_D(t) - k_{FRET} N_D(t) - k_{Lasing\_D} N_D(t) \quad (1)$$

$$dN_A/dt = k_{FRET} N_D(t) - k_A N_A(t) - k_{Lasing\_A} N_A(t) \quad (2)$$

where $N_D(t)$ and $N_A(t)$ are the populations of the excited states of **COPV2** and **COPV3**, respectively; k_{Lasing_D} and k_{Lasing_A} are the rate constants of lasing from **COPV2** and **COPV3**, respectively; and k_D and k_A are the rate constants of the sum of spontaneous emission and nonradiative decay of **COPV2** and **COPV3**, respectively. For realizing FRET-assisted lasing from energy accepting **COPV3**, the following conditions have to be satisfied; (i) $k_{FRET} > k_D$, (ii) $k_{FRET} > k_{Lasing\_D}$, and (iii) $k_{Lasing\_A} > k_A$. PL decay experiments indicate that k_D (= $1/\tau_D$) and k_A are 1.8×10^9 and 8.0×10^8 (s^{-1}), respectively. In the present case, k_{Lasing_D} (= 4.0×10^{10}) is much faster than k_{FRET} and k_D; therefore, conditions (i) and (ii) are not satisfied. Furthermore, k_{FRET} is at the same level as k_D, which also disturbs efficient FRET. Accordingly, to realize FRET lasers, much-faster FRET within the order of several picoseconds is required. One possible way to enhance k_{FRET} is to increase the mixing ratio of A in the co-crystal. However, in the present system, f_{COPV3} levels off at around 0.13 (Figure 1i), and further increase of the mixing ratio of **COPV3** results in a formation of ill-defined aggregates, not well-defined microcrystals (Figure S7). Another strategy to realize FRET lasing is to reduce P_{th} of A while satisfying $k_{Lasing\_A} > k_A$. This condition would induce FRET before lasing from D with low pumping fluence and subsequent lasing from A before spontaneous emission from A.

In this regard, we find a way to reduce P_{th} by controlling the orientation of the microcrystals on a substrate. Microcrystals prepared by the slow evaporation of solvent mostly stick onto the quartz substrate with face-on geometry. This configuration causes a certain degree of leakage of confined light from the microcrystal to the substrate, which possibly results in optical loss and leads to an increase in P_{th}. We noticed that a drop-cast of the solution of **COPV2** on a quartz substrate coated with 50 nm thick rough Ag film results in vertically grown microcrystals

E

by a similar preparation procedure with edge-on geometry (Figures 5a and S16). Upon femtosecond pumping to a standing microcrystal of **COPV2**, lasing occurs with P_{th} of ~8.0 μJ cm^{-2}, which is 4-fold smaller than the value obtained from microcrystals on a quartz substrate with face-on geometry (Figure 5b,c). Similarly, vertically grown co-crystals of **COPV2** and **COPV3** and microcrystals of **COPV3** show P_{th} values 2–4-fold smaller in comparison with the corresponding microcrystals lying on the substrate (Figure 5d). The confinement effect is enhanced by reducing the contact area with the substrate, in addition to the possible mirror effect of the Ag layer.[30] The degree of the reduction of P_{th} is greater than the difference of the absorption cross-section between the microcrystals with face-on and edge-on geometries. Although this method does not reduce P_{th} of only A for FRET lasers, reduction of P_{th} is practically important for enhancing the efficiency of optically pumped lasing.

In summary, rhombic plate-like microcrystals of highly photostable π-conjugated carbon-bridged oligo-phenylenevinylenes (COPVs) are prepared by bottom-up surface self-assembly on a substrate. The resultant microplatelets act as optical resonators with lasing action by optical pumping. Co-crystals with energy-donating and -accepting COPVs display FRET upon weak photoexcitation. However, upon strong pumping, the co-crystals exhibit lasing without FRET, and the rate constant of lasing is 20 times greater than that of FRET. By the changing of the doping level of the energy-accepting COPV, both single- and dual-color lasing is achieved. Vertically grown microcrystals are obtained on a Ag-covered substrate in which the lasing threshold is reduced by one-fourth from that of the microcrystal with a face-on orientation. This study proposes that the control of excited-state kinetics with ultrafast FRET materials is a possible way to realize FRET lasers from organic resonators.

■ ASSOCIATED CONTENT

ⓢ Supporting Information

The Supporting Information is available free of charge on the ACS Publications website at DOI: 10.1021/acs.nanolett.8b01442.

> Additional details on materials and measurements; sample preparation; the apparatus setup; photoabsorption and PL spectra; and SEM, XRD, FDTD simulation, spectroscopic ellipsometry, AFM, time-resolved PL, and transient absorption spectra. (PDF)
>
> Single crystal data of **COPV2** (CIF)

■ AUTHOR INFORMATION

Corresponding Author

*E-mail: yamamoto@ims.tsukuba.ac.jp.

ORCID ⊙

Hayato Tsuji: 0000-0001-7663-5879

Eiichi Nakamura: 0000-0002-4192-1741

Cyriaque Genet: 0000-0003-0672-7406

Thomas W. Ebbesen: 0000-0002-3999-1636

Yohei Yamamoto: 0000-0002-2166-3730

Notes

The authors declare no competing financial interest.

■ REFERENCES

(1) Samuel, I. D. W.; Turnbull, G. A. *Chem. Rev.* **2007**, *107*, 1272–1295.

(2) Venkatakrishnarao, D.; Chandrasekar, R. *Adv. Opt. Mater.* **2016**, *4*, 112–119.

(3) Venkataramudu, U.; Annadhasan, M.; Maddali, H.; Chandrasekar, R. *J. Mater. Chem. C* **2017**, *5*, 7262–7269.

(4) Wang, C. S.; Chen, Y. L.; Lin, H. Y.; Chen, Y. T.; Chen, Y. F. *Appl. Phys. Lett.* **2010**, *97*, 191104.

(5) Cerdán, L.; Enciso, E.; Martín, V.; Banuelos, J.; López-Arbeloa, I.; Costela, A.; García-Moreno, I. *Nat. Photonics* **2012**, *6*, 621–626.

(6) Galisteo-López, J. F.; Ibisate, M.; López, C. *J. Phys. Chem. C* **2014**, *118*, 9665–9669.

(7) Shi, X.; Tong, J.; Liu, D.; Wang, Z. *Appl. Phys. Lett.* **2017**, *110*, 171110.

(8) Sun, Y.; Shopova, S. I.; Wu, C.-S.; Arnold, S.; Fan, X. *Proc. Natl. Acad. Sci. U. S. A.* **2010**, *107*, 16039–16042.

(9) Zhang, X.; Lee, W.; Fan, X. *Lab Chip* **2012**, *12*, 3673–3675.

(10) Wu, X.; Chen, Q.; Sun, Y.; Fan, X. *Appl. Phys. Lett.* **2013**, *102*, 203706.

(11) Koschorreck, M.; Gehlhaar, R.; Lyssenko, V. G.; Swoboda, M.; Hoffmann, M.; Leo, K. *Appl. Phys. Lett.* **2005**, *87*, 181108.

(12) Zhu, X.; Tsuji, H.; López Navarrete, J. T.; Casado, J.; Nakamura, E. *J. Am. Chem. Soc.* **2012**, *134*, 19254–19259.

(13) Morales-Vidal, M.; Boj, P. G.; Villalvilla, J. M.; Quintana, J. A.; Yan, Q.; Lin, N.-T.; Zhu, X.; Ruangsupapichat, N.; Casado, J.; Tsuji, H.; Nakamura, E.; Díaz-García, M. A. *Nat. Commun.* **2015**, *6*, 8458.

(14) Burrezo, P. M.; Lin, N.-T.; Nakabayashi, K.; Ohkoshi, S.; Calzado, E. M.; Boj, P. G.; Díaz-García, M. A.; Franco, C.; Rovira, C.; Veciana, J.; Moos, M.; Lambert, C.; López Navarrete, J. T.; Tsuji, H.; Nakamura, E.; Casado, J. *Angew. Chem., Int. Ed.* **2017**, *56*, 2898–2902.

(15) Quintana, J. A.; Villalvilla, J. M.; Morales-Vidal, M.; Boj, P. G.; Zhu, X.; Ruangsupapichat, N.; Tsuji, H.; Nakamura, E.; Díaz-García, M. A. *Adv. Opt. Mater.* **2017**, *5*, 1700238.

(16) Morales-Vidal, M.; Quintana, J. A.; Villalvilla, J. M.; Boj, P. G.; Nishioka, H.; Tsuji, H.; Nakamura, E.; Whitworth, G. L.; Turnbull, G. A.; Samuel, I. D. W.; Díaz-García, M. A. *Adv. Opt. Mater.* **2018**, 1800069.

(17) Nakanotani, H.; Saito, M.; Nakamura, H.; Adachi, C. *Adv. Funct. Mater.* **2010**, *20*, 1610–1615.

(18) Nakanotani, H.; Adachi, C. *Adv. Opt. Mater.* **2013**, *1*, 422–427.

(19) Sasaki, F.; Mochizuki, H.; Zhou, Y.; Sonoda, Y.; Azumi, R. *Jpn. J. Appl. Phys.* **2016**, *55*, 04ES02.

(20) Zhang, Q.; Su, R.; Liu, X.; Xing, J.; Sum, T.-C.; Xiong, Q. *Adv. Funct. Mater.* **2016**, *26*, 6238–6245.

(21) Kim, S.-S.; Kim, Y.-J.; Yi, G.-C.; Cheong, H. *J. Appl. Phys.* **2009**, *106*, 094310.

(22) Liu, Y.; Dong, H.; Sun, S.; Liu, W.; Zhan, J.; Chen, Z.; Wang, J.; Zhang, L. *Nanoscale* **2013**, *5*, 4123–4128.

(23) Nagawa, M.; Hibino, R.; Hotta, S.; Yanagi, H.; Ichikawa, M.; Koyama, T.; Taniguchi, Y. *Appl. Phys. Lett.* **2002**, *80*, 544.

(24) Kabe, R.; Nakanotani, H.; Sakanoue, T.; Yahiro, M.; Adachi, C. *Adv. Mater.* **2009**, *21*, 4034−4038.

(25) Dong, H.; Zhang, C.; Lin, X.; Zhou, Z.; Yao, J.; Zhao, Y. S. *Nano Lett.* **2017**, *17*, 91−96.

(26) Alvarado-Rodriguez, I.; Yablonovitch, E. *J. Appl. Phys.* **2002**, *92*, 6399.

(27) Oki, O.; Kushida, S.; Mikosch, A.; Hatanaka, K.; Takeda, Y.; Minakata, S.; Kuwabara, J.; Kanbara, T.; Dao, T. D.; Ishii, S.; Nagao, T.; Kuehne, A. J. C.; Deschler, F.; Friend, R. H.; Yamamoto, Y. *Mater. Chem. Front.* **2018**, *2*, 270−274.

(28) Ibisate, M.; Galisteo-López, J. F.; Esteso, V.; López, C. *Adv. Opt. Mater.* **2013**, *1*, 651−656.

(29) Liao, Q.; Jin, X.; Zhang, H.; Xu, Z.; Yao, J.; Fu, H. *Angew. Chem., Int. Ed.* **2015**, *54*, 7037−7041.

(30) Kushida, S.; Okada, D.; Sasaki, F.; Lin, Z.-H.; Huang, J.-S.; Yamamoto, Y. *Adv. Opt. Mater.* **2017**, *5*, 1700123.